European Journal of Pharmaceutical Sciences 105 (2017) 19–32

Contents lists available at ScienceDirect

European Journal of Pharmaceutical Sciences

journal homepage: www.elsevier.com/locate/ejps

Impact of dose and surface features on plasmatic and liver concentrations of biodegradable polymeric nanocapsules

Líliam Teixeira Oliveira[a,b,1], Mônica Auxiliadora de Paula[a,1], Bruno Mendes Roatt[b], Giani Martins Garcia[a,b], Luan Silvestro Bianchini Silva[a], Alexandre Barbosa Reis[b], Carina Silva de Paula[c], José Mário Carneiro Vilela[d], Margareth Spangler Andrade[d], Gwenaelle Pound-Lana[a,1], Vanessa Carla Furtado Mosqueira[a,b,c,*]

[a] *Laboratório de Desenvolvimento Galênico e Nanotecnologia – CiPharma – Programa de Pós-graduação em Ciências Farmacêuticas, Escola de Farmácia, Universidade Federal de Ouro Preto, 35400-000, Minas Gerais, MG, Brazil*
[b] *NUPEB – Núcleo de Pesquisa em Ciências Biológicas, Universidade Federal de Ouro Preto, Campus Morro do Cruzeiro, Ouro Preto 35400-000, Minas Gerais, MG, Brazil*
[c] *Programa de Pós-graduação em Nanotecnologia Farmacêutica em Rede, Escola de Farmácia, Universidade Federal de Ouro Preto, Minas Gerais, MG, Brazil*
[d] *CETEC SENAI – Centro Tecnológico Departamento Regional de Minas Gerais, Avenida José Cândido da Silveira, 2000, Horto, Belo Horizonte 31035-536, Minas Gerais, Brazil*

ARTICLE INFO

Chemical compounds studied in this article:
AlClPc
[chloro(29*H*,31*H*-phthalocyaninato)aluminium (Pubchem CID 123667)
ZnPc [zinc(II) phthalocyanine] (Pubchem CID 2735172)
Poly(D,L-lactide) (PLA Mw 75,000–120,000 g/mol, Pubchem SID 135022784)
Chitosan (75–85% deacetylated, low molecular weight, Pubchem CID 71853)
Pluronic® F68 (Pubchem CID 24751)
Soy lecithin (Epikuron™ 170, Pubchem CID 57369748)
Polyethylene glycol-*block*-poly(D,L-lactide) (PLA-PEG, Pubchem CID 125226)

Keywords:
Nanocapsules
PLA-PEG
Chitosan
Polymer dose
Phthalocyanine
Field flow fractionation

ABSTRACT

The effect of polymeric nanocapsule dose on plasmatic and liver concentrations 20 min after intravenous administration in mice was evaluated. Nanocapsules were prepared with different polymers, namely, poly(D,L-lactide) (PLA), polyethylene glycol-*block*-poly(D,L-lactide) (PLA-PEG), and PLA with chitosan (PLA-Cs) and compared with a nanoemulsion. These formulations were labelled with a phthalocyanine dye for fluorescent detection. The nanostructures had narrow size distributions upon separation by asymmetric flow field flow fractionation with static and dynamic light scattering detection, with average hydrodynamic diameters in the 130–300 nm range, negative zeta potentials, except PLA-Cs nanocapsules, which had a positive zeta potential. Flow cytometry revealed uptake mostly by monocytes and neutrophils in mice and human blood. PLA nanocapsules and the nanoemulsion showed dose-dependent plasma concentrations, where the percentage of plasmatic fluorescence increased with increasing administered dose. In contrast, PLA-PEG nanocapsules led to a dose-independent plasmatic profile. PLA-Cs nanocapsules showed the lowest plasmatic and liver levels of fluorescence at all administered doses and significant intravenous toxicity in mice. This work demonstrates the importance of considering the nanocarrier dose when evaluating pharmacokinetic and biodistribution data and emphasizes the role of surface features in determining the plasmatic and liver concentrations of a poorly soluble lipophilic encapsulated compound.

1. Introduction

Colloidal polymeric nanocarriers, particularly those made of biodegradable polymers, have been extensively investigated as drug delivery systems (Frank et al., 2015). Among these, polymeric nanocapsules (NC, Fig. 1) consist of an oily core surrounded by a polymeric wall (Legrand et al., 1999). Through careful design and selection of the NC components and preparation method for a given drug, such reservoir systems were able to improve the efficacy and reduce the toxicity, thus increasing the therapeutic index of drugs (Legrand et al., 1999; Leite et al., 2007; Mora-Huertas et al., 2010). In order to protect the lipophilic core and to control the release of lipophilic drugs, different

* Corresponding author at: Laboratório de Desenvolvimento Galênico e Nanotecnologia (LDGNano) - Escola de Farmácia, Campus Universitário Morro do Cruzeiro S/N- Universidade Federal de Ouro Preto, 35400-000, Minas Gerais, MG, Brazil.
E-mail address: mosqueira@ef.ufop.br (V.C.F. Mosqueira).
[1] These authors contributed equally.

http://dx.doi.org/10.1016/j.ejps.2017.04.017
Received 12 January 2017; Received in revised form 19 April 2017; Accepted 21 April 2017
Available online 22 April 2017
0928-0987/

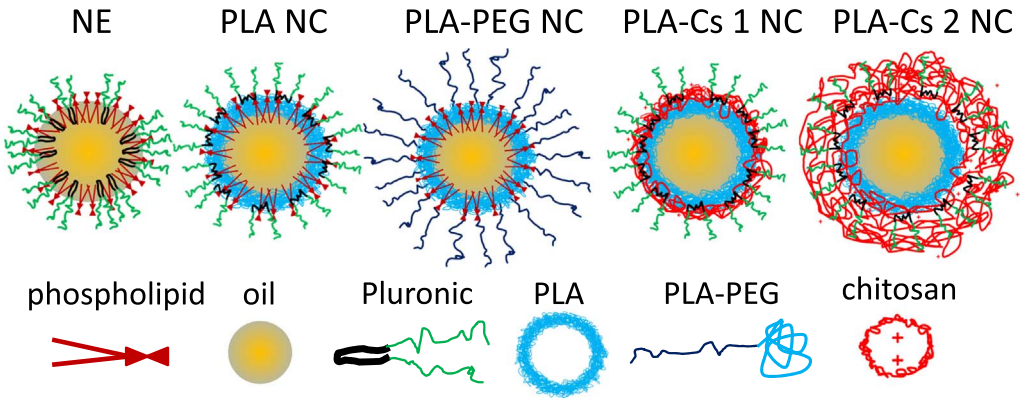

Fig. 1. Schematic representation of the nanostructures.

polymers have been used, such as the biodegradable polymer poly(D,L-lactide) (PLA) and its derivatives. PLA produces a hydrophobic layer at the NC interface, which induces extensive opsonization *in vivo* (Owens and Peppas, 2006) and uptake by the mononuclear phagocytic system (MPS) (Bertrand and Leroux, 2012). Surface modification of the NC with polyethylene glycol (PEG) chains is a successful strategy to improve targeting to other pathological tissues and to extend blood circulation times, particularly using amphiphilic diblock copolymers of PLA with PEG (PLA-PEG). PEG provides a stable steric barrier that reduces opsonization, complement activation and phagocytic uptake (D'Addio et al., 2012; Gref et al., 2000; Gref et al., 1994; Mosqueira et al., 2001b). Another approach is to increase the hydrophilicity of the NC surface by coating with a carbohydrate based-hydrophilic polymer, for instance chitosan (Calvo et al., 1997; Park et al., 2010).

Few studies have been published in the literature, which report an effect of the administered dose of polymeric biodegradable nanoparticles on their pharmacokinetics and biodistribution. Panagi et al. (2001) demonstrated that an increase in the administered dose of radiolabelled poly(lactide-*co*-glycolide) (PLGA) nanoparticles resulted in an increase in the percentage of radioactivity detected in the plasma and liver, whereas the radioactivity blood levels and liver uptake were not affected by the administered dose of PLGA–PEG nanoparticles. Moreover, the elimination rate constant, biological half-life and total body clearance were dose-dependent in the case of the PLGA nanoparticles, whereas they did not depend significantly on the dose in the case of PLGA–PEG nanoparticles.

In comparison with nanospheres, polymeric NC have been little investigated with respect to factors influencing their biodistribution. In particular, the literature lacks data regarding the effect of the administered polymeric dose without variation in NC size. Natural and synthetic polymers with different chemical composition, macromolecular architecture and molar mass have been used as the NC wall-forming polymers. These characteristics are known to dramatically influence the physicochemical properties and stability of the polymeric NC in biological media (Rodriguez-Emmenegger et al., 2011), their *in vitro* behaviour (Mendes et al., 2015), toxicity (Bender et al., 2012; Bulcao et al., 2015) and biodistribution (Vicente et al., 2014; Zhao et al., 2014).

An understanding of the effect of the polymeric dose and physicochemical characteristics of polymeric NC on their plasma/liver distribution is important for a rational therapeutic development. Therefore, in the present study, the effect of the administered dose (*iv*) of PLA NC, PLA-PEG NC and PLA-Cs NC on plasmatic and liver concentrations was investigated and compared with those of a nanoemulsion (NE). The NE was included in the study to evaluate the role of the polymeric capsule wall, considering that the NE only differed from the NC by the absence of a polymeric wall. For this purpose NC and NE formulations were developed and loaded with a phthalocyanine dye (AlClPc) as a fluorescent marker located at the NC core (de Paula et al., 2013). The formulations were thoroughly characterized in terms of nanoparticle size and shape by dynamic light scattering (DLS), asymmetric flow field flow fractionation (AF4) and atomic force microscopy (AFM), surface charge by laser Doppler anemometry coupled to microelectrophoresis, dye encapsulation and release. The interaction of the NC with leukocytes from mice and human whole blood was investigated *ex vivo via* flow cytometry and *in vitro* cytotoxicity was tested on a murine macrophage cell line at different concentrations. The levels of fluorescence were quantified in plasma and liver samples obtained 20 min after intravenous administration of the dye-loaded NC or NE at different doses in healthy mice. The effect of the administered dose is discussed in the light of the physicochemical, *in vitro* and *ex vivo* data, providing experimental basis for the selection of polymeric stabilizers and nanocarrier development.

2. Methods

2.1. Materials

AlClPc [chloro(29*H*,31*H*–phthalocyaninato)aluminum, dye content 85%], ZnPc [zinc(II) phthalocyanine, dye content 97%], poly(D,L-lactide) (PLA, Mw 75,000–120,000 g/mol), 75–85% deacetylated low molecular weight chitosan, Pluronic® F68 (Pluronic), HPLC grade acetone, methanol, ethyl acetate and dimethylformamide used for HPLC analyses and 3-(4,5-dimethylthiazol-2-yl)-2,5-diphenyltetrazolium bromide (MTT reagent) and ethylenediaminetetraacetic acid disodium salt (EDTA) were purchased from Sigma-Aldrich (Sigma-Aldrich Co., St. Louis, MO, USA). Soy lecithin (Epikuron™ 170) was a gift from Cargill (Germany). Poly(D,L-lactide)-*block*-poly(ethylene glycol) (PLA-PEG, *Mn* 66,000 g/mol with a 5000 g/mol PEG block) was as a gift from Alkermes (Massachusetts, USA). Miglyol® 812 N was purchased from Sasol Germany GmBH. Milli-Q water was purified using a Symplicity® System (Millipore, Bedford, USA). The AlClPc dye and AlClPc-loaded formulations were protected from exposure to direct light throughout the experiments.

2.2. Preparation of fluorescent nanocapsules and nanoemulsion

The NC were prepared by the method of polymer deposition followed by solvent displacement, first described by Fessi et al., (1989) modified to obtain AlClPc-loaded NC as in Oliveira et al. (2011). Briefly, the polymer (PLA, 60 mg), the oil (Miglyol 812 N, 250 µl) and soy lecithin (Epikuron™ 170, 75 mg) were dissolved in acetone (30 ml) at 40 °C and AlClPc in ethanol (1 ml of a solution at 1 mg/ml) was added. The solution was poured into the aqueous phase (60 ml of Milli-Q water), containing Pluronic® F68 (75 mg) under moderate magnetic stirring. The suspension was kept under magnetic stirring for 10 min. The solvents were partially evaporated under reduced pressure at 40 °C to a final volume of 10 ml (Heidolph Rotary

Evaporator, Germany). PLA-PEG NC were prepared by substituting PLA by PLA-PEG (75 mg) and in the absence of Pluronic or any surfactant in the aqueous phase. For the preparation of PLA-Cs 1 NC and PLA-Cs 2 NC, the organic phase was composed of PLA (25 mg) and Miglyol 812 N (250 µl) dissolved in 30 ml acetone combined with AlClPc in ethanol (1 ml of a solution at 1 mg/ml). Chitosan (10 mg and 25 mg for PLA-Cs 1 NC and PLA-Cs 2 NC, respectively) was dissolved in 0.05 M aqueous acetic acid and the volume completed to 60 ml with Milli-Q water. Upon complete dissolution of chitosan, Pluronic® F68 (75 mg) was added and the same procedure as described above was followed. The NE was prepared using the same methodology as for PLA NC, omitting PLA. The final polymer concentrations were 6 mg/ml PLA in PLA NC; 7.5 mg/ml PLA-PEG in PLA-PEG NC; 2.5 mg/ml PLA and 1.0 mg/ml chitosan in PLA-Cs 1 NC and 2.5 mg/ml PLA and 2.5 mg/ml chitosan in PLA-Cs 2 NC. The influence of the chitosan to PLA ratio, solvent volume, use of soy lecithin and replacement of part of the acetone by ethanol on NC size (Fig. 2) were evaluated through the preparation of blank NC (no AlClPc added). In all cases a constant ratio of 1:2 (v/v) organic to aqueous phase was used. To administer high doses of NC or NE in an acceptable volume, the formulations were concentrated under reduced pressure to a final volume of 2.5 ml. Prior to administration in mice, PLA-Cs NC were dialyzed using a 14,000 Da cut-off cellulose dialysis membrane in Milli-Q water to remove excess acetic acid.

2.3. Nanoparticle characterization

2.3.1. Particle size and zeta potential determination

The intensity-weighted (*Z*-average) hydrodynamic diameter (D_h) and polydispersity index (PdI) of the formulations at appropriate dilution in ultra-pure Milli-Q water were determined by DLS using a PN3702 Zetasizer Nano ZS (Malvern Instrument, UK) equipped with a He-Ne Laser at 633 nm, set on 173° backscattering mode, at 25 °C. D_h and PdI were calculated by the Zetasizer 7.11 software (Malvern) using the Stokes-Einstein equation with cumulants analysis considering values of 0.8872 cP for water viscosity and 1.330 for water refractive index. NE and NC zeta potentials were determined by laser Doppler anemometry coupled to microelectrophoresis on the same equipment used for DLS analyses, in disposable folded capillary Zeta cells, after dilution at 1:1000 in Milli-Q water.

2.3.2. Atomic force microscopy

Morphological evaluation of the polymeric NC was performed using AFM. The analyses were performed in air at room temperature, on a Dimension 3000 equipment monitored by a Nanoscope IIIa controler from Digital Instruments (Santa Barbara, CA, USA). A 5 µl droplet of NC sample previously diluted in Milli-Q water (1:100) was deposited and spread over the surface of a freshly cleaved mica support and dried under a stream of argon. The images were obtained in tapping mode using commercial Si probes from Nanosensors with cantilevers having a length of 228 µm, resonance frequencies of 75–98 kHz, spring constants of 3.0–7.1 N/m, nominal tip curvature radius of 5 nm to 10 nm and at a scan rate of 1 Hz. Dimensional analyses were performed with the Nanoscope 5.31r1 "section analyses" software. Geometrical diameters were measured on the height images considering the width of the spheres at half height and are reported as the average of values obtained from 40 particles.

2.3.3. Asymmetric flow field flow fractionation

NC and NE fractionation was performed on a Postnova analytics (Landberg, Germany) AF2000 MT AF4 system equipped with a PN7520 solvent degasser, two PN1130 HPLC pumps (tip and focus pumps) and AF2000 module (crossflow pump), PN5300 autosampler, PN4020 Channel oven at 25 °C, a separation channel fitted with a Postnova AF2000 MT Series NovaRC AQU 5 kDa cut-off regenerated cellulose membrane and a 350 µm spacer. The following detectors were placed in series: a PN3211 UV detector with absorbance at 254 nm, a PN3621 multi-angle laser light scattering (MALLS) detector with a 532 nm laser (7°–164°, 21 angles) at 35 °C and a Malvern PN3702 Zetasizer Nano ZS (Malvern Instruments, UK) DLS detector with a 633 nm laser, a Hellma Analytics Suprasil® 3 mm light path quartz flow cell, 173° backscatter detection recorded at 3 s time intervals. The carrier liquid was Milli-Q water filtered on 0.1 µm. The detector flowrate was 0.5 ml/min. NC or NE formulations were diluted in Milli-Q water (1:5) and 10 to 50 µl were injected. The injection flow was set at 0.3 ml/min with injection time of 1.0 min. Variable initial crossflow rates were applied to suit the injected sample type, which were 1.0 ml/min for PLA-Cs NC, 2.0 ml/min for NE and PLA-PEG NC and 2.5 ml/min for PLA NC. The crossflow rate was set to decrease exponentially after a transition time of 1.0 min (except for PLA-Cs NC, where a transition time of 0.2 min was used) from its initial value to 0 over a period of 15 to 60 min. Particle radii of gyration (R_g) were determined in flow mode using the angular variation of the scattered light intensity at angles 12°–164° recorded on the MALLS detector using the Postnova AF2000 software calculation for spherical shape model. The hydrodynamic radii (R_h) were determined in flow mode using the Malvern Zetasizer 7.11 data analysis software. R_g- and R_h-intensity weighted distribution averages were calculated using the UV signal intensity as a measure of the frequency of each fraction and considering only data points within the portion of the peak for which the UV signal intensity was equal to or above 50% of its maximum. This was necessary in order to obtain reliable data, since the sample concentration in the fractions out of this area was too low for accurate flow measurement of R_h *via* DLS. The average dimensionless ratio (R_g/R_h) of a formulation was calculated as the ratio of the calculated average R_g to the average R_h.

2.4. Fluorescent dye quantification by HPLC-FLU

The analytical and bioanalytical methods used to quantify AlClPc, the fluorescent marker used to label the NC and extracted from NC and biological samples, were previously developed and validated by our research group (Oliveira et al., 2011). The HPLC-FLU system consisted of a Waters Alliance 2695 separation module composed of an autosampler, a quaternary pump, column oven set at 35 °C and Waters 2475 fluorescence detector (λ_{ex} 610 nm, λ_{em} 675 nm). The separation was performed on a 150 mm × 4.6 mm, 4-µm particle size C18 Gemini® Phenomenex column protected by an AJO-7597 2 mm × 4.6 mm, 3 µm C18 Phenomenex SecurityGuard™ cartridge. The isocratic mobile phase consisted of a mixture of methanol/acetone/dimethylformamide (80:15:5 v/v/v). It was prepared daily, degassed before use and applied at 1 ml/min. The injection volume was 10 µl. The analytical calibration curve was constructed by linear regression of the plot of the AlClPc peak area against the corresponding concentration range from 0.025 to 5.0 µg/ml.

For the quantification of AlClPc in plasma samples, 10 µl of ZnPc (5 µg/ml in ethanol) as the internal standard (I.S.) were added to each plasma sample (80 µl). The fluorescent dye was extracted with 1 ml of ethyl acetate, shaken on a vortex for 10 min and centrifuged at 9300 × *g* for 10 min. This procedure was repeated 3 times and the resulting upper organic layers were pooled, filtered (0.45-µm Millex) (Millipore, USA), evaporated to dryness under a nitrogen stream and finally reconstituted with 100 µl of the HPLC mobile phase. For quantification in liver samples, 200 mg of liver (200 mg) were homogenized for 1 min in a round-bottom plastic tube with 1 ml of sodium phosphate buffer (pH 6.5) at room temperature in an ultrasonic processor (Vibra cell™ VC750) with a metal rod titanium probe at 300 W. AlClPc was extracted from 80 µl of the homogenate tissue using the same procedure described above for plasma samples and reconstituted with 100 µl of the mobile phase and assayed by HPLC-FLU. The bioanalytical curves covered a concentration range of 15–100 ng/ml for plasma and 75–500 ng/g for the liver. Calibration curves were constructed by linear least-squares regression analysis by plotting the peak-area ratios (AlClPc/I.S.) *versus* the drug concentrations. The coefficients

of correlations of the calibration curves were all greater than or equal to 0.98.

2.5. Percentage of dye encapsulation

The colloidal suspensions were filtered using a 0.8 μm filter (Durapore, Millipore®) to remove potential aggregates. The filtrate (100 μl) was added to 2.5 ml of acetonitrile (to disrupt the NC and release AlClPc), vortexed for 5 min, and centrifuged at 500 × *g* for 30 min. The total AlClPc in the colloidal suspension was determined in the supernatant by HPLC-FLU (Section 2.4). Another 400 μl of the filtrate were submitted to ultrafiltration in an AMICOM device (Microcon Ultrafilter, MWCO 50,000 Da, Millipore®) at 500 × *g* for 20 min (de Paula et al., 2013) to separate AlClPc associated with nanostructures from free AlClPc (non-encapsulated). AlClPc associated with the nanostructures was retained in the upper compartment of the device. Acetonitrile (200 μl) was added to 50 μl of the ultrafiltrate and the sample submitted to HPLC-FLU for the quantification of the non-encapsulated AlClPc (free AlClPc). All samples were filtered using a 0.45 μm filter and 25 μl were injected in the HPLC-FLU system. The analyses were performed in triplicate. The percentage of AlClPc-loading in NE and NC (Table 1) was calculated as the difference between the total AlClPc in the colloidal suspension and the free AlClPc in the aqueous phase divided by the total AlClPc in the colloidal suspension, in percentage.

2.6. AlClPc solubility studies

The thermodynamic solubility of AlClPc in phosphate buffered saline (PBS) at pH 7.4 was determined at 37 °C to establish *sink* conditions (up to 20% of the saturation concentration) for further *in vitro* release study. An excess of AlClPc (10 mg in 1 ml of PBS) was weighed and allowed to equilibrate with the solution for 48 h. The tubes were centrifuged at 2000 × *g* for 10 min and an aliquot of 500 μl was collected, filtered and placed in an Eppendorf tube containing 500 μl of methanol, vortex-mixed and analysed by HPLC-FLU using the conditions described above.

2.7. In vitro release kinetics

The *in vitro* release studies of AlClPc encapsulated in NC and NE were performed in PBS (pH 7.4) by direct dialysis. AlClPc-loaded NC or NE (360 μl of formulation at 0.1 mg/ml AlClPc) were placed in a 14,000 Da cut-off cellulose dialysis tubing, sealed and immersed in a glass beaker containing 500 ml of release medium. The entire system was kept at 37 °C under mild stirring. At predetermined time intervals, aliquots (500 μl) were withdrawn from the external solution and an equal amount of fresh PBS was added to maintain a constant volume. Methanol (500 μl) was added, the samples were vortex-mixed, centrifuged at 2000 × *g* for 10 min and the supernatants (25 μl) were injected for HPLC-FLU analysis. AlClPc release in n-octanol was performed under sink conditions, as previously described by de Paula et al. (2013). Aliquots of 0.5 ml of NE and PLA-Cs NC (0.1 mg/ml of AlClPc) were placed in a centrifuge tube with 1.5 ml of n-octanol, in triplicate. The tubes were immersed in a water bath at 37 °C under agitation. At predetermined time intervals, the tubes were withdrawn and centrifuged at 2000 × *g* for 5 min. The organic layer was withdrawn (100 μl) and diluted in 900 μl of acetonitrile. The amount of AlClPc released at each timepoint was determined by HPLC-FLU.

2.8. Ex-vivo interaction of NC with peripheral blood mononuclear cells of mice and humans by flow cytometry

The interaction of NC with peripheral blood mononuclear cells was studied by flow cytometry. EDTA-venous blood samples were collected from healthy mice (n = 4) and healthy humans (n = 2) following approved ethical protocols no. 2014/20 and no. 2009/29 (UFOP, Brazil). Aliquots (100 μl of the whole blood) were mixed with 10 μl of AlClPc-loaded NC (PLA NC, PLA-PEG NC or PLA-Cs 2 NC) and incubated in the absence of light at 37 °C for 2 h. As control, 100 μl of the whole blood was incubated with 10 μl of NC diluent. Subsequently, the total blood cell samples were washed with PBS (pH 7.4) and centrifuged to remove unbound nanoparticles. After lysis of the erythrocytes with 1% BD FACS Lysing solution the samples were centrifuged at 600 × *g* for 7 min at room temperature. The supernatant was discarded and the pellet containing leukocytes washed with 3 ml of PBS (pH 7.4) and centrifuged under the same centrifugation conditions as above. The samples were analysed immediately after by flow cytometry on a FACScalibur® - Becton Dickinson instrument equipped with an excitation laser line at 488 nm and a 635 nm (argon-ion lasers) for detection of fluorescence emission at 488 and 661 nm, respectively. The phenotypic and morphometric parameters of the cells present in each tube were determined. The program CELLQuest® (Franklin Lakes, NJ, USA) was used for data acquisition and analysis of results from 20,000 events/sample. Data were analysed as a linear equivalent mean fluorescence channel histogram. The phagocytic index was calculated as the ratio of the mean fluorescence intensity for each cell type to the percentage of such cells in the whole blood.

An additional experiment was performed using Transwell® devices (0.1 μm pores, Sigma) in 24-well cell culture plates with the different NC labelled with AlClPc. Whole blood (3.15 ml) was placed in each well and 350 μl of NC formulation in the upper compartment of the Transwell device. The Transwells were immersed in the plates containing blood and incubated at 37 °C for 0.25–2 h. No direct contact between NC and cell was possible. Blood was analysed by flow cytometry as described above.

2.9. Cytotoxicity assay

The J774A.1 murine macrophage-like cell line (ATCC® TIB-67™) was maintained as an adherent culture in humidified atmosphere (5% CO_2/95% air) at 37 °C in Roswell Park Memorial Institute (RPMI) medium (Lonza) containing phenol red, 4.5 g/l of glucose and L-glutamine, supplemented with 10% (v/v) foetal bovine serum (FBS) (Cultilab), penicillin (100 IU/ml) and streptomycin (0.1 mg/ml solubilized in citrate buffer). For experiments, cells were detached mechanically with a cell scraper (Biofil) and adjusted to the required concentration of viable cells by counting in a Neubauer chamber in the presence of trypan blue. J774A.1 cells were plated at a concentration of 12,500 cells per well in 96-well plates (Sarstedt, Brazil). After 12 h of

Table 1
Physicochemical characteristics of the fluorescently labelled nanostructures.

Formulation	NE	PLA NC	PLA-PEG NC	PLA-Cs 1 NC	PLA-Cs 2 NC
D_h (nm) (*PdI*)	133 ± 1 (*0.15*)	181 ± 2 (*0.19*)	203 ± 1 (*0.11*)	248 ± 5 (*0.15*)	297 ± 1 (*0.19*)
ζ (mV)	− 36.0 ± 0.2	− 44 ± 4	− 35 ± 1	+ 25.6 ± 0.3	+ 26.5 ± 0.2
Dye encapsulation (%)	> 99.8	> 99.8	> 99.8	> 99.8	> 99.8

D_h mean hydrodynamic diameter by batch dynamic light scattering, PdI Polydispersity index, ζ zeta potential, mean values ± standard deviation. The fluorescent marker AlClPc was loaded at a concentration of 0.1 mg/ml.

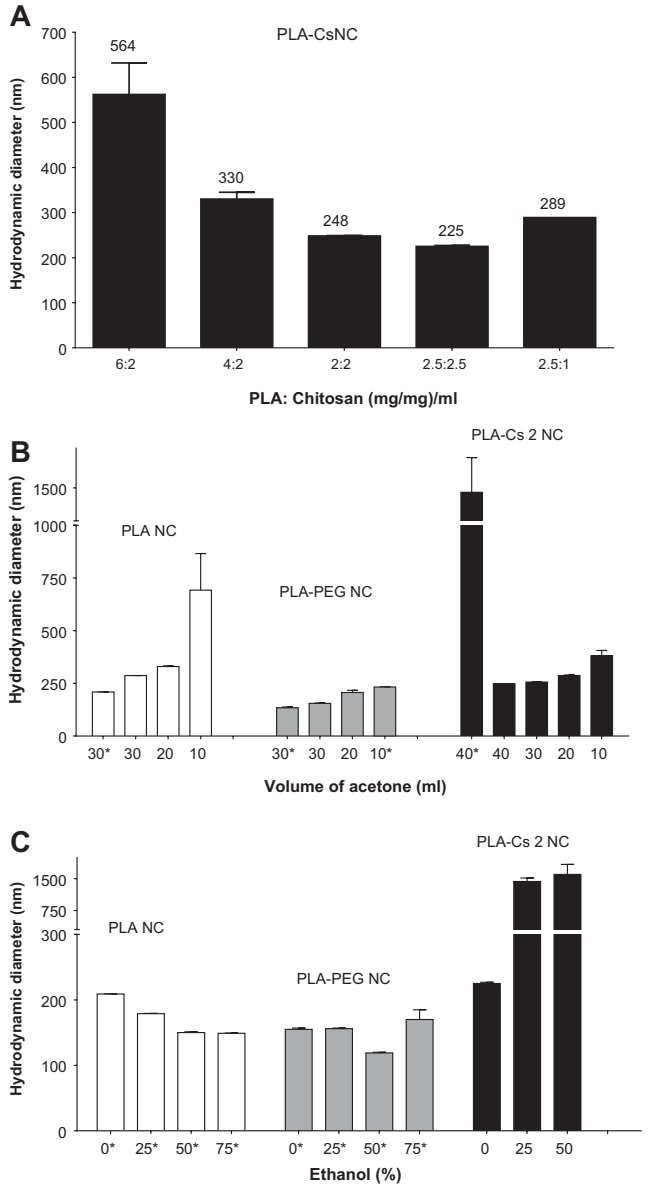

Fig. 2. Factors affecting nanocapsule size. Effect of polylactide (PLA) and chitosan content (A), solvent volume (B) and proportion of ethanol in the organic phase (v/v) (C) on the hydrodynamic diameter of blank polymeric nanocapsules of PLA (open bars), PLA-PEG (grey bars) or PLA with chitosan (black bars).*Formulations prepared using lecithin.

adherence, the medium was removed and the wells were washed once with PBS (Lonza) containing Ca^{2+} and Mg^{2+} to remove non-adherent cells. The cells were incubated for 24 h with the different NC formulations diluted in complete medium at polymer concentrations of 1, 5, 10, 50, 100 and 500 µg/ml. The medium was removed and the cells were washed twice, to remove excess NC, with PBS containing Ca^{2+} and Mg^{2+} to guarantee adhesion of live cells. The MTT reagent (200 µl of a solution at 0.5 mg/ml in RPMI with 10% v/v FBS) was added to each well and the plates were incubated for 4 h at 37 °C (5% CO_2/95% air), centrifuged, the medium discarded and 200 µl of dimethyl sulfoxide were added to solubilize the formazan crystals formed. The absorbance was determined on an ELISA plate reader (Molecular Devices®) at 570 and 650 nm. Cell viability percentages were calculated as the ratio of the mean absorbance of triplicate readings to the mean absorbance of control wells of three independent experiments.

2.10. In vivo studies

2.10.1. Animals

The *in vivo* experiments were approved by the Ethics Committee on Animal Experimentation of the Universidade Federal de Ouro Preto, Brazil (protocols no. 2009/29 and 2014/20) and are in compliance with the guidelines established by the Brazilian College of Animal Experimentation (COBEA) (Neves et al., 2013). Female Swiss mice weighing 25–30 g were used in this study. They were maintained under the following environmental conditions: 12 h day/night cycles, room temperature of 22 ± 2 °C, standard diet and water *ad libitum*.

2.10.2. Nanoparticle administration and quantification of fluorescent dye in plasma and liver

AlClPc-loaded NC and NE were filtered through a Millex HV (Millipore®) 0.8 µm filter and an aliquot was taken to determine the concentration of AlClPc in the volumes administered to animals by HPLC-FLU. The mice received a single intravenous dose of NC over a dose range of 3 to 360 mg of polymer (PLA or PLA-PEG or PLA and chitosan) per kg of animal bodyweight. NE was administered at doses equivalent to those of PLA NC with respect to all other ingredients (Miglyol 812N, soy lecithin, Pluronic F68 and AlClPc). Twenty min upon intravenous administration of the formulations, blood (150 µl) was collected in heparinized tubes. The blood samples were immediately centrifuged for 10 min at 400 × *g*, and plasma separated from cells and frozen at − 80 °C until analysis. The mice were euthanized and the livers excised, washed with cold saline and blotted with filter paper. The quantification of AlClPc in biological samples was undertaken within 12–24 h post-collection of the samples using the method described in Section 2.4.

NC and NE surface areas (m^2) were calculated as previously described (Mosqueira et al., 1999) based on the mean hydrodynamic diameter of the particles measured by DLS in batch (Table 1) and the volume of the constituents in the formulations. The total volume of NE or NC per ml of the colloidal suspension is given by the sum of the volumes of oil, polymer and lecithin, considering densities of 1.2 g/cm^3 for PLA and chitosan, 1.26 g/cm^3 for PLA-PEG and 1.0 g/cm^3 for soy lecithin. The number of particles in each formulation was calculated dividing the total particle volume by the volume of one particle.

2.11. Statistical analysis

Statistical analyses were performed using GraphPad Prism® (Prism 6.01 for Windows). One-way ANOVA for multiple comparisons was used, followed by a parametric *t*-test with Bonferroni multiple comparison post-test for *ex-vivo* data. The *in vivo* dose-response curves were analysed by linear and nonlinear regression and R^2 values were used to evaluate the goodness of fit. The zeta potential, nanoparticle sizes and cytotoxicity data were compared using paired student *t*-test. All data are expressed as mean ± SD. A *p*-value of 0.05 or less was indicated as statistically significant.

3. Results

3.1. Particle size, size-dispersity and zeta potential analysis

Polymeric NC, which differ in their surface chemistries (Fig. 1), were prepared *via* the interfacial deposition of preformed polymers followed by solvent displacement, a method first reported by Fessi et al. (1989). This method was slightly modified to prepare chitosan-coated PLA NC (PLA-Cs NC). PLA-Cs NC 1 and 2 differ only by the amount of chitosan used in their preparation, namely a 1:1 (w/w) ratio of PLA to chitosan in PLA-Cs 1 NC *versus* 1:0.4 in PLA-Cs 2 NC. Process parameters, such as the volume of organic and aqueous phases, the proportion of polymers, and ethanol content were optimized in order to obtain nanoparticles with a mean hydrodynamic diameter lower than

300 nm and polydispersity index (PdI) lower than 0.3 (Fig. 2), considered suitable for intravenous administration.

For all NC types, increasing the volume of the organic solvent decreased significantly ($p < 0.05$) the average size of the NC (Fig. 2). Addition of soy lecithin to the organic phase significantly reduced the size and dispersity of PLA NC ($p < 0.05$) and produced PLA-PEG NC with diameters lower than 300 nm, whereas a significant increase in particle size ($p < 0.05$) was observed for PLA-Cs NC. In the absence of lecithin a 1:1 or 1:0.4 (w/w) ratio of PLA to chitosan polymers at a concentration of 2.5 mg/ml of PLA were suitable to produce particles with a diameter lower than 300 nm and PdI lower than 0.3 (Fig. 2 and Table 1).

Labelling of the NC with the fluorescent marker AlClPc for *in vitro* and *in vivo* studies was achieved concomitantly to particle formation, as previously described (de Paula et al., 2013). Ethanol was evaluated as a water- and acetone-miscible organic phase component, which was required as a better solvent for AlClPc than acetone. The addition of ethanol in the organic phase increased significantly the particle size in the case of PLA-Cs NC (Fig. 2). Therefore the lowest possible amount of ethanol was used to solubilize AlClPc while keeping the particle size lower than 300 nm.

The NE, PLA and PLA-PEG NC had negative zeta-potentials with values in the range of −35 to −44 mV, whereas NC containing chitosan had positive zeta potentials (Table 1) attributed to chitosan association with the NC surface. Increasing the chitosan content 2.5-fold did not affect significantly the PLA-Cs NC zeta potential but produced NC with a slightly larger mean hydrodynamic diameter, as seen when comparing PLA-Cs 1 and PLA-Cs 2 NC (Table 1).

3.2. Fluorescent dye encapsulation

The concentrations of AlClPc determined in the ultrafiltrate of the colloidal suspensions were lower than the quantification limit of the method (Oliveira et al., 2011). Consequently, percentages of dye encapsulation close to 100% were obtained (Table 1).

3.3. Atomic force microscopy

The AFM images show that all NC produced have a spherical shape with differences in their organization and morphology depending on their composition (Fig. 3). The determined mean geometrical diameters of PLA, PLA-PEG, PLA-Cs 1 and PLA-Cs 2 NC were 164 nm, 231, 183 and 265, respectively, with vertical distances of 40–80 nm, indicating flattening of the NC during the analysis. PLA-Cs 2 NC prepared with the higher content of chitosan induced technical difficulties in AFM analysis and complex images with low definition of the spherical structures were produced (Fig. 3). PLA-Cs 1 and PLA-Cs 2 NC exhibited differences in their morphological features in AFM images and their mean geometrical diameters increased significantly with the increase in chitosan content ($p < 0.05$) (Fig. 3). PLA-Cs 2 NC appeared to be immersed in a matrix. In contrast, PLA-Cs 1 NC presented a better defined spherical structure, particularly in the phase image.

3.4. Asymmetric flow field flow fractionation

The NE and NC were successfully fractionated by AF4, as indicated by an increase in the hydrodynamic radius (R_h) of each fraction with increasing retention time (Fig. 4). For chitosan-containing samples a lower initial crossflow (1 ml/min) was necessary compared to other samples. Higher initial cross-flow values resulted in unpractically long retention times (> 50 min), most likely due to ionic interaction with the cellulose membrane. Size-dependent elution of the chitosan-containing samples was observed under our experimental conditions, in spite of their positive surface charge. Other authors reported the requirement of a cationic-modified cellulose membrane and low pH buffered carrier liquid in order to minimize electrostatic interaction with the negatively-charged regular cellulose membrane (Ma et al., 2010), which were not necessary in our case. The particle size distribution parameters are reported in Table 2. PLA-PEG NC had the lowest size-dispersity (R_h ranging from 87 to 127 nm) and PLA-Cs 1 NC the highest (R_h ranging from 102 to 242 nm). In particular, 90% of the UV signal in AlClPc-loaded NE, PLA and PLA-PEG NC corresponded to particles with D_h lower than 300 nm, whereas > 55% of the signal from PLA-Cs 1 NC and 50% of PLA-Cs 2 NC corresponded to particles with D_h above 300 nm.

3.5. Release study

The solubility at equilibrium of the AlClPc dye in PBS pH 7.4 at 37 °C was 363.95 ng/ml. The release profiles in PBS were similar between all types of NC and NE, consisting of a rapid and limited burst release followed by a sustained phase. The percentage of AlClPc released from NC in PBS during the burst phase depended on the nature of the stabilizing polymer and decreased in the order PLA-Cs NC < PLA NC < PEG-PLA NC < NE with values of 27, 22, 16 and 5%, respectively (Fig. 5 (top) and Table 3). The AlClPc dissolution rate (K_d) and the apparent release rate from the nanocarriers (K_{app}) were calculated (Table 3). The rate of dye release in n-octanol was lower for all formulations than in PBS (Fig. 5 (bottom) and Table 3). During the burst phase NE showed a percentage of released AlClPc significantly lower than that of the NC in both PBS and n-octanol, and significantly higher release during the sustained phase for up to 24 h (insert in Fig. 5).

3.6. Ex-vivo interaction of NC with peripheral blood mononuclear cells of mice and humans

The interaction of the NC with leukocytes from peripheral blood from healthy humans and mice was evaluated by flow cytometry. Close to 100% of lymphocytes, monocytes and neutrophils showed associated fluorescence upon incubation with fluorescently labelled NC for 2 h (Fig. 6), indicating that the leukocytes present in the whole blood interact with PLA, PLA-PEG and PLA-Cs 2 NC in a way that leads to stable surface binding and/or endocytosis. Monocytes and neutrophils showed significantly higher fluorescence intensities than lymphocytes (Fig. 6). The phagocytic index was calculated for each cell and particle type, in order to normalize for the relative abundance of each leukocyte type in blood and thus give a better reflection of the amount of associated particles per cell. Monocytes had the highest phagocytic index (350–650, depending on the formulation type), indicating that they are the main cells in blood responsible for the interaction with polymeric NC. Neutrophils, which are the most abundant leukocytes (55%) had a phagocytic index of 20–56, approximately ten-fold lower than monocytes and not significantly different ($p > 0.05$) from that of the lymphocyte population.

No differences in the phagocytic index of human monocytes, lymphocytes or neutrophils with the three types of NC tested were observed in human blood ($p > 0.05$). In contrast, in mice blood, a significantly lower phagocytic index was observed with PLA-Cs 2 NC for leukocytes, in particular monocytes, compared to those obtained with PLA NC and PLA-PEG NC.

3.7. Nanocapsule cytotoxicity assay

The J774A.1 murine macrophage-like cell line incubated for 24 h with PLA, PLA-PEG and PLA-Cs 2 NC showed cell viability higher than 70% up to the concentration of 100 μg/ml (insert in Fig. 7). From concentrations of 100 μg/ml to 500 μg/ml cell viability underwent a sharp drop to < 5%, 10% and 50% for PLA NC, PLA-PEG NC and PLA-Cs 2 NC, respectively. The polymer concentration of 500 μg/ml showed cytotoxicity for all tested NC. At this polymer concentration the cell viability was significantly higher for PLA-Cs 2 NC than for PLA and

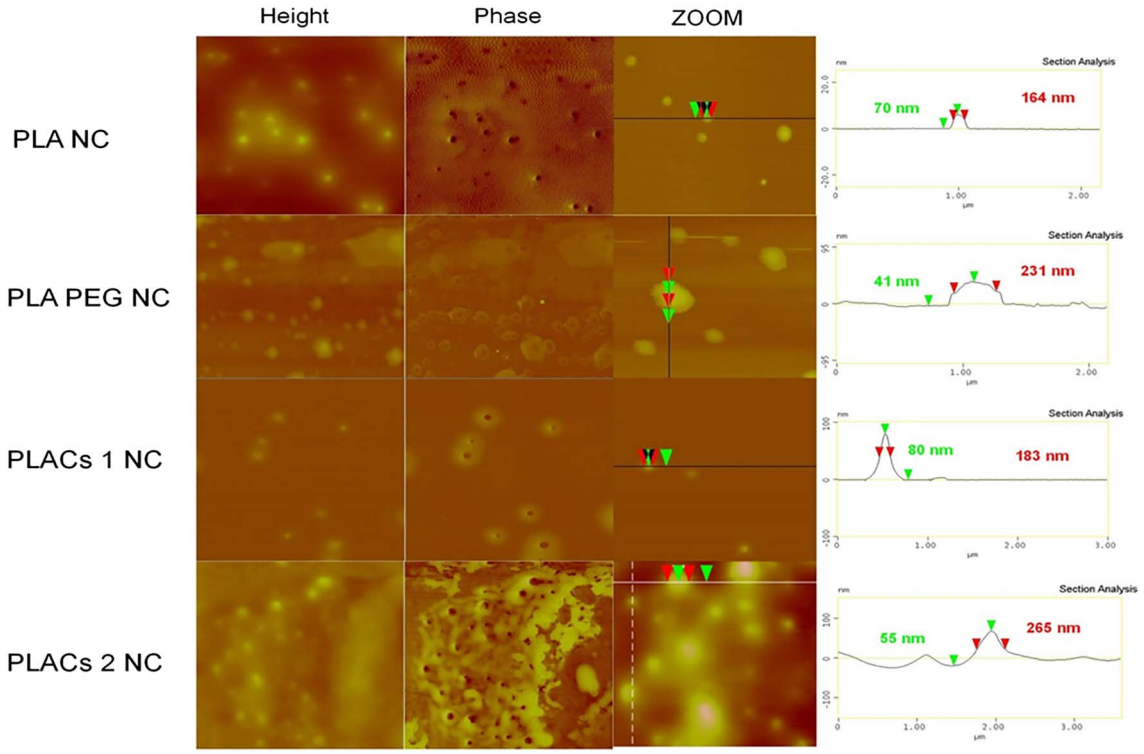

Fig. 3. Atomic force microscopy images of the nanocapsules. Height and phase images with scan size 3 × 3 μm for PLA and PLA-PEG NC and 5 × 5 μm for PLA-Cs NC, Z range 250 nm in height and 30° in phase images for all formulations. Section analysis performed on zoom images.

PLA-PEG NC. However, when expressed as a function of the particle number per ml, the threshold for cell toxicity was significantly lower with PLA-Cs 2 NC ($> 550 \times 10^6$) than with PLA ($> 7000 \times 10^6$) or PLA-PEG NC ($> 6000 \times 10^6$) (Fig. 7).

3.8. In vivo dose effect study

The plasmatic and liver levels of fluorescence 20 min after intravenous administration and in particular the dose-related evolution of the plasmatic concentrations varied dramatically from one type of nanoparticle to the other (Fig. 8). For both NE and PLA NC, the proportion of the administered fluorescence detected in the plasma increased with administered dose. Significantly higher values ($p < 0.05$) were obtained for NE than for PLA NC. The percentage of administered fluorescence detected in the plasma was constant with PLA-PEG NC. Translated into absolute values, this means that within the administered dose range studied, the levels of fluorescence in the plasma followed a linear increase as a function of the administered dose of PLA-PEG NC. In contrast, both PLA-Cs NC showed a decrease in the percentage of fluorescence detected in the plasma with increased administered dose. No significant differences between PLA-Cs 1 NC and PLA-Cs 2 NC data were observed ($p > 0.05$). Acute toxic effects were observed upon administration of PLA-Cs NC at doses higher than 160 mg/kg, which include dyspnoea, tachycardia, prostration and sudden death in some animals. Blood collected from an animal treated with PLA-Cs NC at the dose of 160 mg/kg had higher viscosity than normal and showed haemolysis. These observations suggest acute toxicity related to thromboembolic events, which lead to rapid death of mice. These signs of toxicity were not observed with NE, PLA NC or PLA-PEG NC.

An increase in the administered doses of all formulation types led to a dose-dependent decrease in the percentage of the administered fluorescence detected in the liver. In the liver similar dose-response profiles ($p > 0.05$) were obtained with PLA and PLA-PEG NC, whereas NE and both PLA-Cs NC showed significantly lower liver percentages. Similar profiles were observed when data were plotted in terms of the percentages of fluorescence detected in the plasma as a function the total surface area administered per kg of animal bodyweight (Supplementary material).

4. Discussion

4.1. Nanoparticle design

The NC evaluated in the present study all contained PLA as their polymeric wall-forming component, however the hydrophilic polymer selected to stabilize the interface of the NC varied, *i.e.* Pluronic F68 in the case of PLA NC *versus* a PLA-PEG block copolymer in the case of PLA-PEG NC and a combination of Pluronic F68 and chitosan for PLA-Cs NC. The Zeta-potential measurements confirmed the expected surface charge inversion when using chitosan with positive values for PLA-Cs NC, whereas PLA and PLA-PEG NC had negative zeta potentials. This study therefore enables a comparison between polymeric NC with electrostatic stabilization with a negative surface charge (PLA NC), a positive surface charge (PLA-Cs NC) and a combination of steric and electrostatic stabilization with PLA-PEG NC.

The section below discusses formulation requirements identified in order to achieve diameters lower than 300 nm, low PdI and colloidal stability for each type of NC. The use of soy lecithin was an efficient strategy to decrease particle size and provide colloidal stability in PLA and PLA-PEG NC. On the contrary, addition of lecithin to PLA-Cs NC formulations had a detrimental effect on the particle size. Diameters in the micrometre range and higher were obtained for PLA-Cs NC prepared with soy lecithin, as opposed to 230 nm under optimal conditions in the absence of lecithin. It is likely that the negatively charged components of soy lecithin form ionic complexes with the amino groups along the chitosan chains, leading to micrometre-sized aggregates. The increase in viscosity of the system in the presence of chitosan is aggravated by the presence of soy lecithin, also possibly contributing to the increase in size, consequently lecithin was excluded

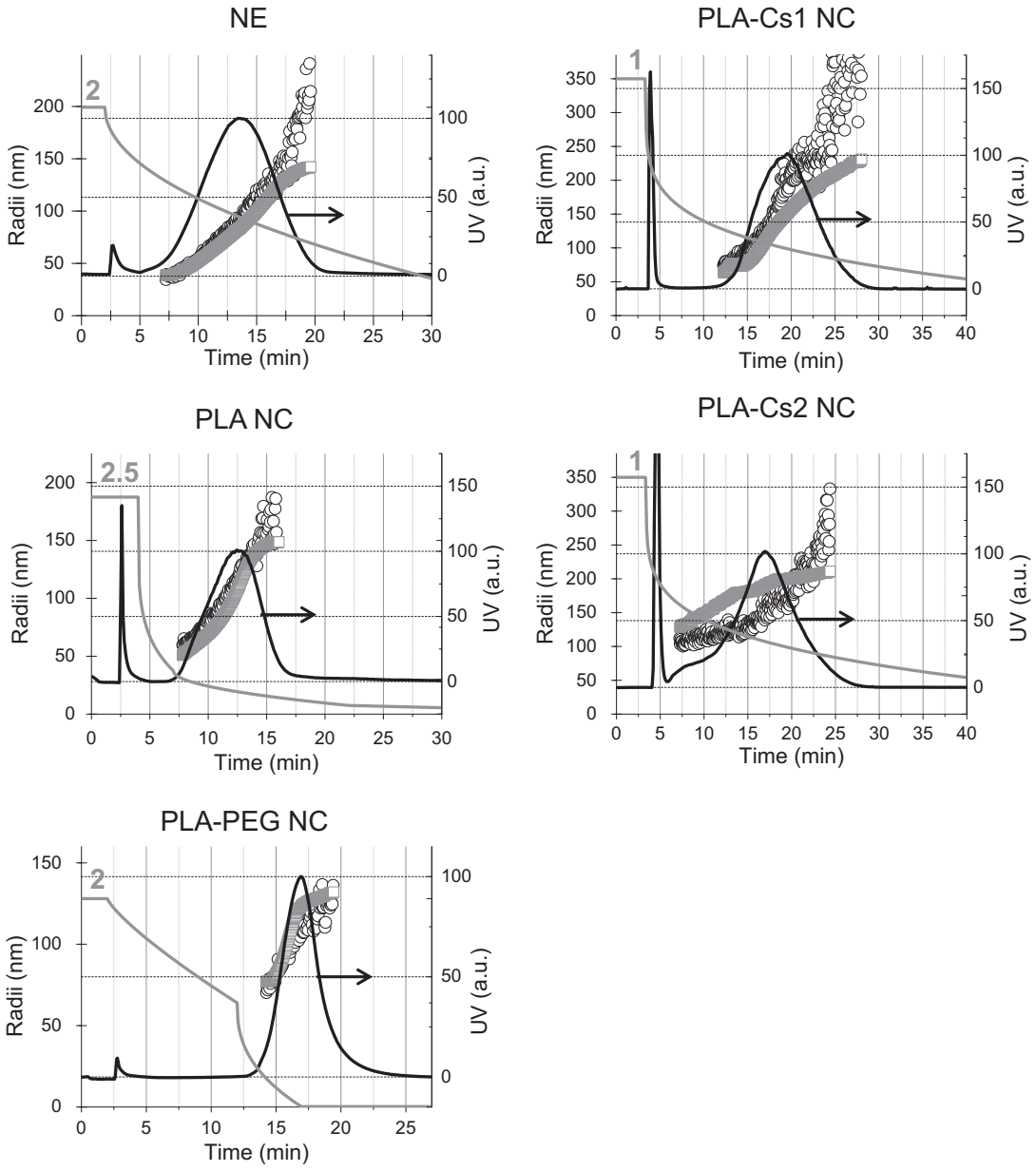

Fig. 4. Asymmetric-flow field flow fractionation of the nanostructures. UV absorption signal (black line, right y-axis), R_g determined by MALLS (grey open squares), R_h determined by DLS (black open circles) and profile of the applied crossflow (grey line, initial crossflow rate indicated in grey font above the curve, in ml/min).

Table 2
Size distribution by asymmetric-flow field flow fractionation.

Formulation	NE	PLA NC	PLA-PEG NC	PLA-Cs 1 NC	PLA-Cs 2 NC
R_g range[a,b] (nm)	53–126	65–143	87–127	81–195	144–203
R_h range[b,c] (nm)	54–143	75–148	87–127	102–242	110–211
Flow R_g[a] average (nm)	106	84	115	108	161
Flow R_h[b] average (nm)	113	94	108	122	119
Average R_g/R_h	0.93	0.92	1.07	0.88	1.34

[a] Gyration radii determined by multi-angle laser light scattering in flow mode.
[b] Values corresponding to the size range (minimum-maximum) of the particles within the portion of the fractionated sample peak which UV signal intensity was higher than 50% of the peak maximum.
[c] Hydrodynamic radii determined by dynamic light scattering in flow mode.

from the preparation of PLA-Cs NC.

The negative zeta potential values obtained in our study for PLA NC and PLA-PEG NC are typically observed for colloidal carriers containing PLA and soy lecithin and can be attributed to superficial anionic groups, mainly due to the negatively charged phosphatidic acid in Epikuron 170 (soy lecithin). The NE, which was prepared under the same conditions as PLA NC but in the absence of PLA, also showed a negative zeta potential, also most likely due to the presence of phosphatidic acid at the oil droplet surface. The PEG corona in PEG-PLA NC decreased the zeta potential in modulus but did not completely mask the negative charge of the core components of the NC, as also observed by Mosqueira et al. (2001a).

Another determining factor in controlling the particle size in NC formulations was the polymer concentration at the time of mixing of the organic phase with the aqueous phases. Reducing the viscosity of the organic phase favours diffusion of the solvent towards the aqueous phase (Lepeltier et al., 2014). As a result the particles have a smaller diameter. Varying the polymer concentration in the organic phase,

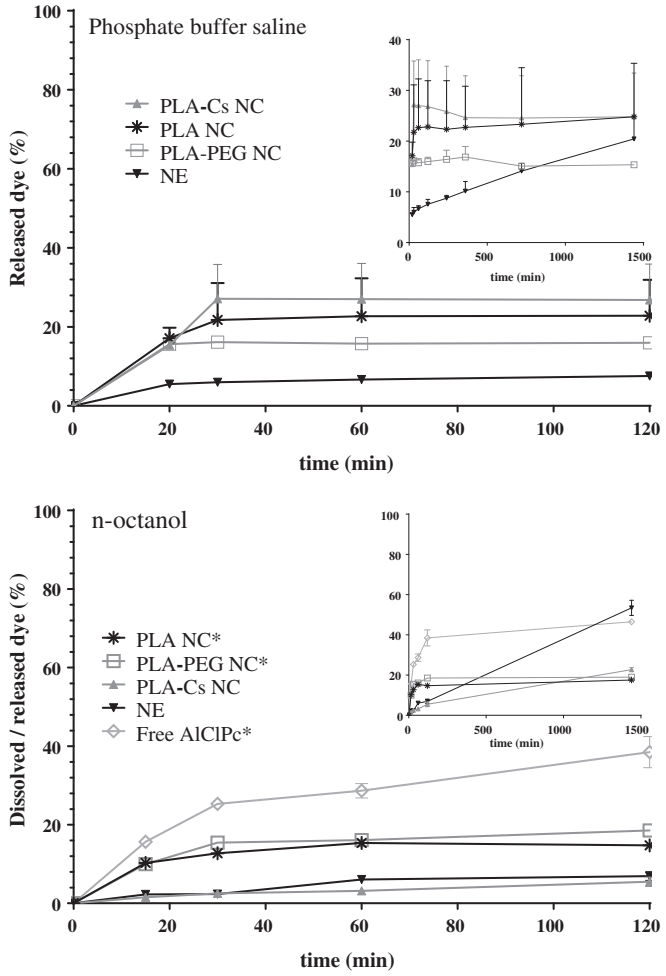

Fig. 5. Release of AlClPc from nanocapsules and nanoemulsion in phosphate buffer saline (top) and in n-octanol (bottom). insert: datapoints at 12 and 24 h. Data is the mean of three independent experiments ± SD (n = 3).

while maintaining the ratio of organic to aqueous phase constant, can therefore be considered a general and straightforward strategy for tuning the size of such types of NC.

4.2. Morphological characterization of the nanoparticles

AFM phase images give valuable information on the tridimensional structure and texture of the NC. AFM analysis in *tapping mode* requires only mild experimental conditions suitable for probing soft samples. Vesicular polymeric nanostructures containing an oily core have already been successfully analysed and their vesicular structure was confirmed by this method (de Assis et al., 2008; Garcia et al., 2015; Leite et al., 2005; Mosqueira et al., 2005; Pereira et al., 2008). Phase images of our NC (Fig. 3) revealed differences in stiffness of the NC core (dark regions) surrounded by a shell (lighter layer). These images confirm that the nanostructures are composed of a core that is probably softer than the external layer. The height images of PLA-PEG NC show a layer surrounding a spherical structure. These layers could correspond to the PEG layer in a "brush" conformation. The particles in PLA-Cs 2 NC appeared to be immersed in a soft matrix surrounding the NC, an interesting aspect of this formulation. Particularly, the phase images show the core that seems to emerge from a chitosan matrix with different stiffness and viscoelasticity. PLA-Cs 1 NC prepared with lower chitosan content showed dramatically different height and phase AFM images, with well-defined spherical particles and no chitosan "cloud" (Fig. 3).

In order to gain a better understanding of some morphological features of these fluorescent dye labelled NC and NE and be able to correlate these physicochemical features to their *in vivo* behaviour, AF4 fractionation with online dual size characterization was carried out. AF4 is a powerful tool to investigate the size-distribution of complex colloids in solution. Sample fractionation with online dynamic and static light scattering determination of R_g and R_h indicated that the AlClPc-loaded particles, although considered of low size-dispersity according to batch DLS measurements, were composed of particles with variable size-dispersity (Fig. 4 and Table 2). The R_g/R_h ratio, the dimensionless ratio or shape factor, obtained by comparing the radii obtained by MALLS and DLS, gives information on the particle shape (spherical *vs* elongated), and on the mass distribution around the centre of mass of the particles. The methodology applied in this study for NC and NE preparation, AFM analyses and previous studies indicate that the NC are spherical. For spherical particles R_g/R_h of 0.775 is characteristic of spheres with uniform density, such as polystyrene latexes (Brewer and Striegel, 2009), values close to 1.0 are obtained with vesicles or hollow spheres (Stauch et al., 2002; Vezočnik et al., 2015), values above 1 are obtained with elongated or porous structures and values as low as 0.3 are characteristic of microgels (Kunz et al., 1983). Taking advantage of the fractionation technique, we calculated the value of R_g/R_h for each fraction within the fractionation peak. The R_g/R_h values of 0.93, 0.92 and 1.07, respectively, indicate that the AlClPc-loaded NE, PLA NC and PLA-PEG NC are vesicular structures. These values are in agreement with literature values for similar types of NC (Roy et al., 2015) and liposomes (Vezočnik et al., 2015). The higher R_g/R_h for PLA-PEG NC may be attributed to the PEG corona creating a dense hydration layer around the oil-polymer vesicle resulting in a density shift towards the outer particle layer. These formulations showed little variation in the R_g/R_h along the size-distribution, indicating homogenous particle morphology across the size distribution. Similar homogeneity in dispersion and structure of PLA-PEG NC was evidenced previously using density gradients (Mosqueira et al., 2001a), and the core-corona structure was evidenced by small angle X-

Table 3
Dissolution of free AlClPc and release of AlClPc loaded in colloidal suspensions in phosphate buffer saline and *n*-octanol.

	Free AlClPc	PLA NC	PEG-PLA NC	PLA-Cs NC	NE
% released in 20 min (PBS)	8.0 ± 0.7	17 ± 3	15.6 ± 0.9	15.4 ± 0.8	5.5 ± 0.4
% released in 15 min (n-octanol)	15.7 ± 0.4	10.3 ± 0.5	10 ± 1	15.6 ± 0.7	2.3 ± 0.3
K_d [a] (PBS) %·min^{-1}	0.054	–	–	–	–
K_d [b] (n-octanol) %·min^{-1}	0.033*	–	–	–	–
K_{app} [c] (PBS) %·min^{-1}	–	0.075	0.199	0.057	0.063
K_{app} [d] (n-octanol) %·min^{-1}	–	0.072*	0.057*	0.011	0.018

[a] K_d (PBS) = dissolution constant of free AlClPc performed in PBS buffer.
[b] K_d (n-octanol) = dissolution constant of free AlClPc performed in n-octanol.
[c] K_{app} (PBS) = apparent dissolution constant of AlClPc from the colloidal suspensions performed in PBS buffer.
[d] K_{app} (n-octanol) = apparent dissolution constant of AlClPc from the colloidal suspension performed in n-octanol.
* De Paula et al., 2013.

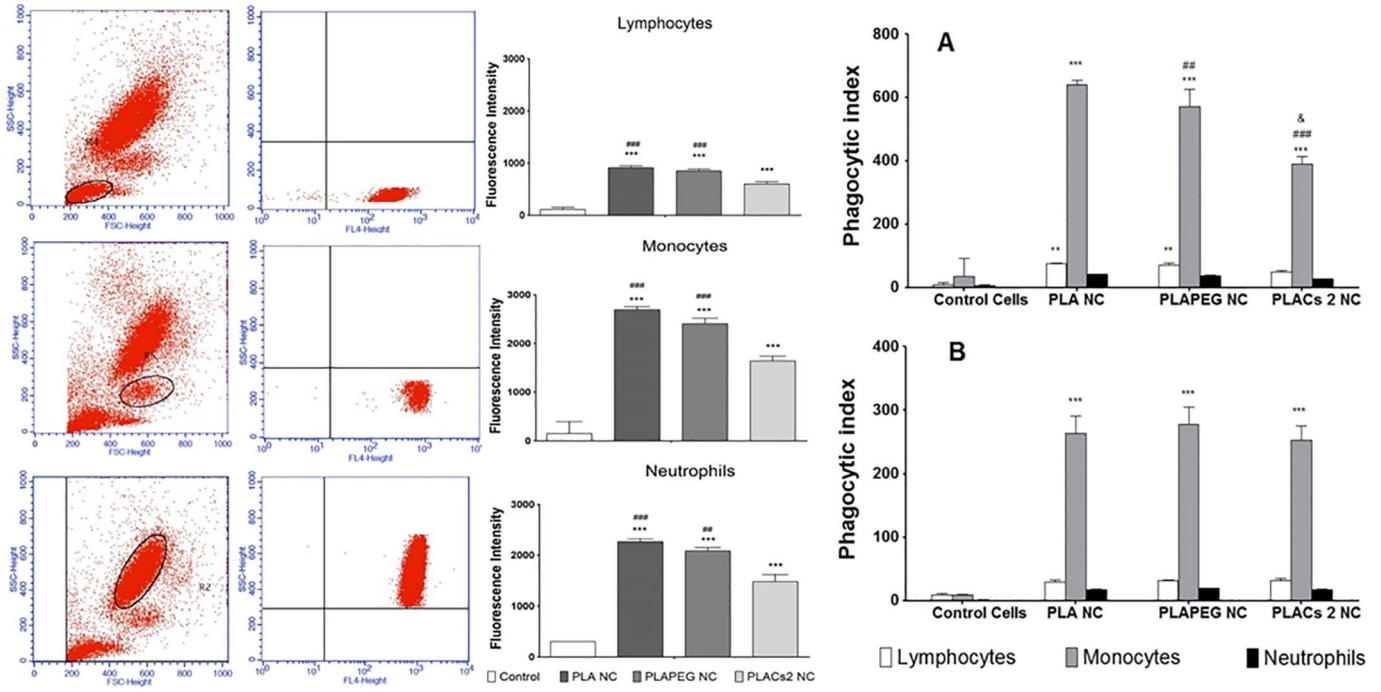

Fig. 6. Flow cytometry analysis of the interaction of NC with blood leukocytes. Phagocytic index of lymphocytes, monocytes and neutrophils in mice (A) and human (B) blood. The cells were incubated with AlClPc-loaded PLA, PLA-PEG and PLA-Cs 2 NC.*$p < 0.05$, **$p < 0.01$ and ***$p < 0.001$ compared to control cells, $^{\#\#}p < 0.01$ and $^{\#\#\#}p < 0.001$ compared to PLA NC and & compared to PLA-PEG NC.

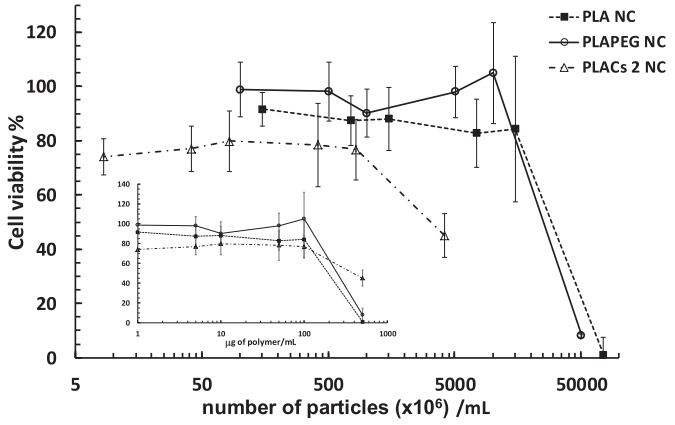

Fig. 7. Effect of polymer concentration or number of nanocapsules on the cytotoxicity against J774A.1 cells. Data is the mean of three independent experiments ± SD (n = 9).

ray analyses on similar systems (Rube et al., 2005). The elution peak of PLA-Cs 2 NC was broader and irregularly shaped compared to the other NC (Fig. 4). For this sample an average R_g/R_h of 1.34 was obtained, similar to that observed by Ma et al. with chitosan-DNA complexes (Ma et al., 2010). For PLA-Cs 2 NC the R_g/R_h ratio was found to be close to 1.5 for the smaller particles and close to 1.0 for the larger particles. Such a non-linear and large variation in the dimensionless ratio is an indication of the heterogeneity of the sample. On the contrary, sample PLA-Cs 1 NC showed an average R_g/R_h of 0.88, and a smaller variation of this ratio over the size-distribution (between 0.9 and 0.6). Similar average D_h were obtained for both samples upon fractionation (D_h = 243 nm for PLA-Cs 1 NC and D_h = 238 nm for PLA-Cs 2 NC). It is possible that PLA-Cs 1 NC, which was prepared with half the amount of chitosan compared to PLA-Cs 2 NC, consisted of denser particles with a chitosan outer layer tightly adsorbed to the surface of the NC, whereas PLA-Cs 2 NC had a loosely adsorbed chitosan outer layer with dangling chitosan chains. This hypothesis is supported by AFM analysis of these samples.

The morphological analyses of PLA-Cs NC therefore suggest that chitosan was present in excess in PLA-Cs 2 NC, the formulation that employed an equal amount of PLA and chitosan. The lower amount of chitosan used for PLA-Cs 1 NC was sufficient to confer a positive surface charge to the NC as well as produce dense spherical nanoparticles, resulted in a more homogeneous formulation and avoided high amounts of loosely adsorbed, soluble or suspended chitosan chains.

4.3. Dye encapsulation and release

AlClPc was selected as a fluorescent marker for the NC and NE for *in vivo* and *ex vivo* studies due to its lipophilic character (CLogP = 7.4, calculated using ChemDraw ultra software 12.0, CambridgeSoft) responsible for its poor aqueous solubility (< 0.4 μg/ml in PBS pH 7.4 at 37 °C, this study). NC and NE have an oily core where a lipophilic compound may be dissolved or dispersed. The high percentages of dye encapsulation obtained in our study confirm association of the dye to the nanostructures. The limited and rapid burst obtained within 30 min in the release profiles of all formulations in PBS suggests that a fraction of encapsulated AlClPc is associated to the surface of the NC. It is expected that the chemical composition of the polymer interface influences the degree of association of a lipophilic compound at the interface. The slower but sustained release from NE suggests that the oily core of the NC and NE is a good medium to solubilize AlClPc and also that the presence of the polymer at the NC interface delays release from the NC core in comparison with NE. On the other hand, the release profiles of AlClPc from NC and NE in *n*-octanol were very slow (Fig. 5), which suggests poor transfer of this dye from nanoparticles to lipophilic membranes. Our release study confirms the literature data with polymeric NC *versus* NE, where sustained release of lipophilic compounds is achieved by the polymeric wall of NC and drug retention is governed by partition between the oily core and the continuous aqueous phase (Cruz et al., 2006; Mosqueira et al., 2006). The use of some organic fluorescent dyes such as Nile Red or Rhodamine B as NP markers is criticized on the basis of their leakage from the NP (Abdel-Mottaleb et al., 2015). In addition to the *in vitro* release study, a preliminary test was carried out to probe fluorescence transfer towards

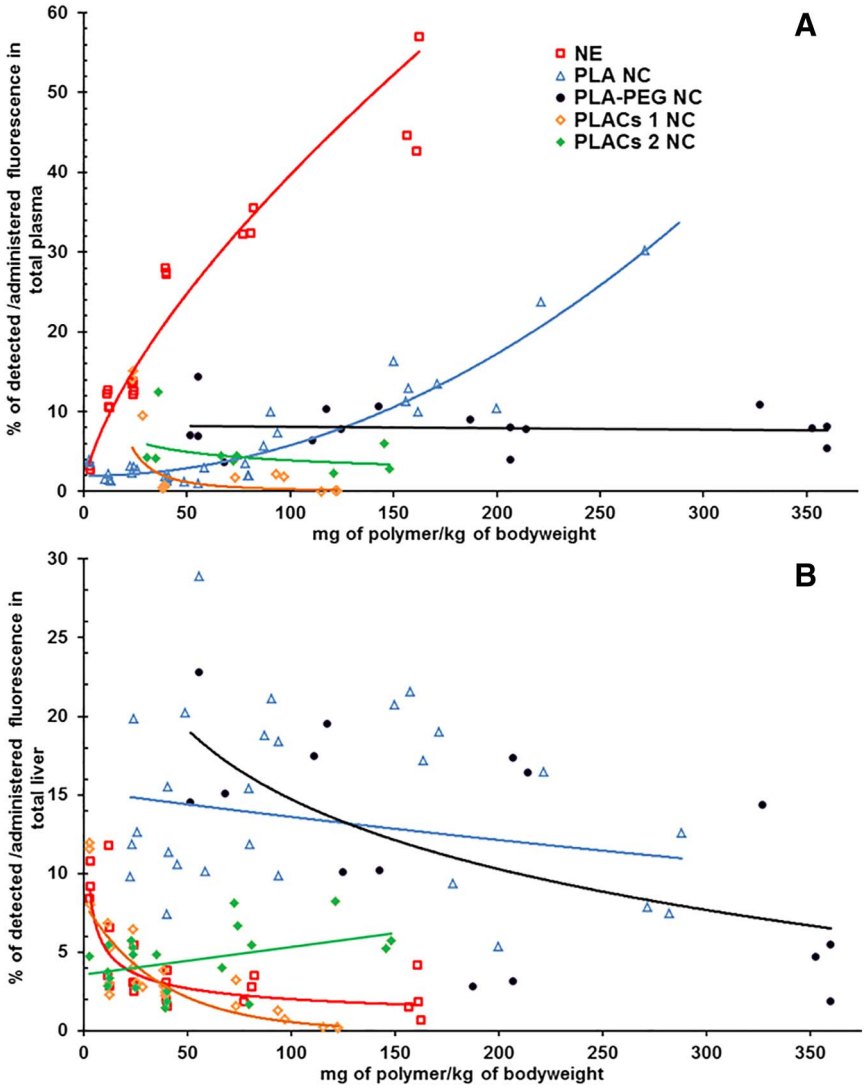

Fig. 8. Effect of nanocarrier administered dose on levels of fluorescence detected in the plasma (A) and liver (B) 20 min after administration. The nanoemulsion (NE), which did not contain any polymeric wall, was administered at doses equivalent to that of PLA NC with respect to all other ingredients. The full lines are best mathematical fits for experimental data.

cells in cell culture medium *via* leakage from the NC. AlClPc-loaded NC were placed in a Transwell® insert with a 0.1 μm pore size and incubated with human blood cells, such that particles were retained in the insert, while soluble components could be exchanged between the cells and particles. After 15 min of incubation fluorescence was not detected in cells incubated with AlClPc-loaded NC.

In conclusion, fluorescence detected in samples from *in vitro* as well as *in vivo* analyses will mostly originate from the uptake of dye-loaded NC or *via* mechanisms that require contact between cells and NCs, rather than the release of the dye from the NC to the medium and further interaction with cells.

4.4. Interaction of the nanoparticles with cells

Blood cells are the first cell type to interact with nanoparticles administered intravenously. Nanoparticles interact with the circulating immune cells and this interaction can induce an immune response. We determined the level of NC uptake by primary immune cells for the different polymeric NC *via* flow cytometry upon incubation of whole blood with NC suspensions for 2 h. Monocytes were the main leukocyte type to interact with all types of NC. The presence of the PEG corona at the NC surface did not result in a decrease in its level of interaction with blood cells, as indicated by similar phagocytic indices for all leukocyte types with either PLA NC or PLA-PEG NC in human blood. These findings are in agreement with a recent study where internalization of PEG-coated lipid NC by immune cells was observed at a similar frequency to Pluronic F68 or chitosan coated PLA NP (Farace et al., 2016). Interestingly, a significantly lower level of interaction of PLA-Cs NC was observed with mice than with human leukocytes in comparison with the other NC. While this observation may correlate with substantial differences in leukocyte characteristics or in immune response between the two species, further experiments would be required to elucidate the origin and impact of such a divergent *in vitro* behaviour and its implications for transposition to *in vivo* human studies.

4.5. In vivo study

Plasmatic and hepatic levels of fluorescence in response to increased administered doses of fluorescent NE followed very different trends in comparison with PLA NC, 20 min after intravenous administration. The 20 min timepoint was selected based on previous pharmacokinetic and biodistribution studies of PEG-PLA and PLA NC, where it was found that at 20 min extensive biodistribution had already occurred (Mosqueira et al., 2001b; Oliveira et al., 2011). In fact, these studies found that in 5 min the total dose in plasma of mice was < 5% of the administered dose. In the range of 12 to 150 mg/kg of animal bodyweight, plasmatic

levels of fluorescence were five to ten times higher with NE than with PLA NC, and the liver levels about ten times lower with NE than with PLA NC. Pharmacokinetics of NE stabilized with Pluronic F68 may involve pathways similar to those of NC, *via* opsonization and uptake by the MPS, or they may behave as physiological chylomicrons and undergo lipolysis (Torcello-Gomez et al., 2014). In our study low levels of fluorescent marker were detected in the liver, suggesting that liver uptake plays little role in blood clearance of the NE droplets in comparison with NC formulations. As opposed to NC, NE do not have a polymeric wall to stabilize them. It is therefore possible that fast interaction of NE with plasma components, particularly lipoproteins, led to transfer of the fluorescent marker or even fusion of the NE droplet with lipoproteins. This fusion would lead to high plasmatic concentrations of the dye shortly after injection and possibly extended plasmatic residence time of the dye. Experimentally it is extremely difficult to separate a dye (or drug) associated to nanocarriers from the free dye associated to plasma components, bound to plasma proteins or transferred to lipoproteins, in particular upon *in vivo* administration. The hypothesis that dyes suffer fast transfer from NE to lipoproteins could not be excluded and could partially explain its limited association to MPS in the liver (Fig. 8). It can be expected that a lipophilic drug or dye, as is the case of AlClPc, would have a comparatively slower rate of transfer from polymeric NC than from NE to the plasma at all doses tested. Release of the dye to the plasma was most exacerbated by an increase in administered dose when loaded in NE in comparison with PLA NC. One hypothesis is that at higher administered dose interaction of the NE with blood components other than blood cells may be favoured. The dramatic difference in the profiles of the plasma-dose curves between NE and PLA NC points at the importance of the polymer in determining the *in vivo* fate of the bioactive compound associated to the NC. In order to achieve controlled drug delivery, slow and controlled release from the nanocarrier to the plasma is a prerequisite and would be desirable to eventually reach the goal of targeted delivery to specific organs.

Significantly higher fluorescence blood levels were obtained with PLA NC than with PLA-PEG NC at administered doses higher than approx. 125 mg (or an estimated 25 m^2)/kg of animal bodyweight, whereas at lower doses the opposite was observed. Mosqueira et al. determined that the clearance rate of PLA NC administered intravenously at a dose of 36 mg/kg of mice bodyweight was higher than those of a PLA-PEG NC by a factor of four to nine, depending on the polymer chain-length (Mosqueira et al., 2001b), in agreement with our results at low administered doses. Panagi and coworkers (Panagi et al., 2001) found that PLGA nanoparticle blood clearance rates were orders of magnitude higher than that of PLA-PEG nanoparticles and more importantly they found that clearance rates were dose-dependent in the case of PLGA nanoparticles but not of PLGA-PEG nanoparticles. Hence, the higher the PLGA nanoparticle administered dose, the lower the clearance rate. These authors also observed that there was no dose-dependency with PLGA-PEG nanospheres. Our data with PLA-PEG NC are in agreement with Panagi's- study. By combining our results with previous experimental findings we can therefore put forward the hypothesis that the high plasmatic percentages obtained with high doses of PLA NC were due to a drastic decrease in plasma clearance rates at increased administered doses. This effect suggests saturation of MPS phenomena or opsonin depletion by PLA NC at high doses.

The similar liver percentages of fluorescence as a function of the administered dose for both PLA NC and PLA-PEG NC suggest that the mechanisms underlying the dose-dependency of the plasmatic concentrations with PLA NC were not merely related to variations in their liver uptake within the administered dose-range studied. Due to the steric stabilization provided by PEG chains, it would be expected that higher levels of opsonization of the PLA NC would occur (Mosqueira et al., 2001a). It is well known that increased doses of liposomes lead to longer circulation times, as already described for non-pegylated liposomes (Allen and Hansen, 1991). This effect is generally believed to result from 'saturation' of macrophages of the MPS, which play a dominant role in the clearance process. The lower percentage of NC uptake by the liver observed in our experiments with increasing PLA and PLA-PEG NC polymeric doses suggests some degree of saturation of the MPS uptake pathways. Higher depletion of blood opsonins or complement consumption would possibly result in a decrease in the liver uptake of PLA NC compared to PLA-PEG NC as a function of an increase in the administered dose, as estimated for similar polymeric nanocarriers (Carlander et al., 2016). However, in the present study, no significant differences in liver uptake between both formulations were observed ($p > 0.05$). Poor correlation between liver levels of fluorescence and administered dose was observed. In our experiment the fluorescence in the liver showed higher inter-individual variation than in the plasma. Therefore further investigation would be required in order to explain the differences between PLA NC and PLA-PEG NC in terms of plasmatic levels and their evolution with increasing dose.

Our *in vitro* experiment with uptake by circulating monocytes and neutrophils from peripheral blood indicated that these cells participate actively in the removal of the NC from the plasma (Fig. 6). The NC remain in the bloodstream, however, associated to these cells. As a consequence, lower uptake of these NC by liver Kupffer cells, the major cell type involved in liver uptake within 20 min, would be expected. In addition, a study conducted with PLA nanospheres administered intravenously to mice at a single high dose (200 mg/kg) found that the phagocytic function, evaluated in terms of the clearance rate of colloidal carbon, was not affected 1 h after administration (Fernández-Urrusuno et al., 1996). This study and ours suggest that even at a dose of polymeric NC that could induce depletion of blood opsonins, the phagocytic index may not be dramatically altered shortly after administration. Circulating leukocytes are rarely contemplated in pharmacokinetic studies with nanoparticles. Our study suggests that these cells play an important role in nanoparticle clearance and biodistribution.

PLA-Cs NC showed the lowest plasmatic percentages and the lowest uptake by the liver, regardless of the administrated dose. Since the pKa of the amino groups of chitosan is 6.4, at physiological pH (7.3–7.4) they are in their deprotonated form, providing less electronic repulsion between nanoparticles and lower hydrophilicity than at lower pH. Farace et al. (2016) found that chitosan NC aggregated upon immersion in buffer at pH 7.4. Similarly, PLA-Cs NC are likely to aggregate under physiological pH. Chitosan in itself is known to be thrombogenic (Balan and Verestiuc, 2014) leading to red blood cell aggregation. In our *ex-vivo* flow cytometry experiment cell lysis was observed upon incubation with PLA-Cs NC, however, the ratio of dead to live cells was not determined. Bender and co-workers (Bender et al., 2012) noted that the degree of haemolysis and platelet aggregation increased with increasing doses of chitosan-coated poly(ε-caprolactone) NC. The potential aggregation of chitosan under physiological condition and a possible increase in haemolysis and platelet aggregation at higher doses of PLA-Cs NC could result in the formation of a thrombus. Shenoy et al. (2005), showed that stealth poly(amino ester) nanoparticles in the size range of 100–200 nm and surface charge of approximately + 30 mV significantly accumulated in the heart and lung tissues. This was correlated with a lower level of accumulation in the liver as compared to that of polyester nanoparticles, as was observed with our PLA-Cs NC. It was suggested that a higher degree of aggregation of the cationic nanoparticles in the presence of serum proteins affected their biodistribution leading to accumulation in the lung. Similarly, pulmonary accumulation of chitosan coated-PLGA nanoparticles was reported (Yang et al., 2009). Our cell viability results showed cytotoxicity of PLA-Cs NC towards the J774.A macrophage cell line at a lower number of NC (or total NC surface area) than of PLA or PLA-PEG NC.

The cytotoxicity of chitosan itself depends on the pH of the cell viability assay medium (Younes et al., 2016), which in the present case was kept at physiological value (7.4). Higher cytotoxicity of PLA-Cs NC may be expected at a lower pH value, where the amino groups of chitosan are protonated and the polymer is more soluble to interact

with cells. A detailed study on chitosan-coated NC in biological media found that PLA-Cs NC aggregation depends not only on chitosan degree of acetylation and pH (an aggravating factor in our study where 75–85% deacetylated chitin was used) but also the type of culture medium composition (Goycoolea et al., 2012). The differences between the formulations observed in our *in vivo* study may be related to cytotoxic effects towards this type of cells. In addition, on the basis of clinical observations, it is likely that the toxicity observed in mice that received doses equal to or above 120 mg/ml of PLA-Cs NC was due to respiratory failure probably caused by pulmonary embolism. We suggest that both experimental outcomes were related to chitosan aggregation under physiological conditions. It is important to note that the plasmatic levels of fluorescence determined in our study do not include the portion of the marker associated to blood cells. However our *ex-vivo* flow cytometry experiment indicates that upon incubation of all NC with whole blood of mice and humans the leukocytes presented fluorescence due to the AlClPc dye. For a better understanding of the *in vivo* fate of the NC it would therefore be interesting to quantify their levels not only in the plasma but also in red blood cells.

An ongoing debate in the literature discusses the prominence of the particle number or surface area rather than the mass of polymer or nanoparticles tested or administered in determining biological behaviours *in vitro* and *in vivo*. When the *in vivo* data were plotted in terms of the percentages of fluorescence detected in the plasma, resp. liver as a function of the total surface area administered per kg of animal bodyweight (Supplementary material) similar profiles to those of Fig. 8 were observed, indicating that within the limits of our study the effects observed could not be attributed merely to variations in the size of the nanoparticles between formulations.

5. Conclusions

For the first time a systematic comparison between NC evidenced the influence of variable surface compositions on the plasmatic and liver levels of a hydrophobic molecule loaded in the nanocarriers in response to increased administered nanocarrier dose. The present *in vivo* study demonstrates the importance of the polymeric wall of NC and its chemical nature in determining the extent to which plasma clearance and liver uptake are affected by the administered dose. Increasing the administered dose appeared to affect significantly the biodistribution of the NE and PLA NC between plasma and liver but it did not appear to affect the plasma profile of the PLA-PEG NC in the range of doses applied here. The effects of nanocarrier surface chemical composition on clearance rates from the plasma are typically reported in the literature at one or two administered doses. The present investigation demonstrates the importance of considering the nanocarrier dose when evaluating such parameters. This work will benefit further experimental and modelling studies on the *in vivo* fate of highly lipophilic cargo in NC towards nanocarrier design and engineering. AlClPc, which we used as a fluorescent dye to label the NE and NC, is a chemical photosensitizer currently under investigation for photodynamic cancer therapy. Therefore, the present AlClPc-loaded NE and NC physicochemical characterization, dye-loading and release studies, and plasma/liver distribution could contribute to the development of AlClPc-based therapeutics.

Supplementary data to this article can be found online at http://dx.doi.org/10.1016/j.ejps.2017.04.017.

Declaration of interest statement

The authors declare no conflict of interest.

Acknowledgements

This work was financially supported by the Brazilian agencies Conselho Nacional de Desenvolvimento Científico e Tecnológico (CNPq, projects # 312893/2009-4 and # 481195/2011-4), Fundação de Amparo a Pesquisa do Estado de Minas Gerais (FAPEMIG, PPM-00452-11 and 00432-13, BPD-00612-14), Coordenação de Aperfeiçoamento de Pessoal de Nível Superior (CAPES, for student bursaries) and NANOBIOMG Network (RED-00007-14) Minas Gerais. We thank Patrícia Capelari at UFOP and Dr. Gerhard Heinzmann and Tony Pfaffe at Postnova Analytics for support with AF4.

References

Abdel-Mottaleb, M.M.A., Beduneau, A., Pellequer, Y., Lamprecht, A., 2015. Stability of fluorescent labels in PLGA polymeric nanoparticles: quantum dots versus organic dyes. Int. J. Pharm. 494, 471–478.
Allen, T.M., Hansen, C., 1991. Pharmacokinetics of stealth versus conventional liposomes - effect of dose. Biochim. Biophys. Acta 1068, 133–141.
de Assis, D.N., Mosqueira, V.C.F., Vilela, J.M.C., Andrade, M.S., Cardoso, V.N., 2008. Release profiles and morphological characterization by atomic force microscopy and photon correlation spectroscopy of 99mTechnetium-fluconazole nanocapsules. Int. J. Pharm. 349, 152–160.
Balan, V., Verestiuc, L., 2014. Strategies to improve chitosan hemocompatibility: a review. Eur. Polym. J. 53, 171–188.
Bender, E.A., Adorne, M.D., Colomé, L.M., Abdalla, D.S.P., Guterres, S.S., Pohlmann, A.R., 2012. Hemocompatibility of poly(ε-caprolactone) lipid-core nanocapsules stabilized with polysorbate 80-lecithin and uncoated or coated with chitosan. Int. J. Pharm. 426, 271–279.
Bertrand, N., Leroux, J.-C., 2012. The journey of a drug-carrier in the body: an anatomo-physiological perspective. J. Control. Release 161, 152–163.
Brewer, A.K., Striegel, A.M., 2009. Particle size characterization by quadruple-detector hydrodynamic chromatography. Anal. Bioanal. Chem. 393, 295–302.
Bulcao, R.P., Bubols, G.B., Nascimento, S.N., Gauer, B., Sauer, E., Baierle, M., Charao, M.F., Moro, A., Brucker, N., Bruinsmann, F.A., Schnorr, C., Moreira, J.C.F., Pohlmann, A.R., Guterres, S.S., Garcia, S.C., 2015. Do poly(epsilon-caprolactone) lipid-core nanocapsules induce oxidative or inflammatory damage after in vivo subchronic treatment? Toxicol. Res. 4, 994–1005.
Calvo, P., Remuñan-López, C., Vila-Jato, J.L., Alonso, M.J., 1997. Chitosan and chitosan ethylene oxide propylene oxide block copolymer nanoparticles as novel carriers for proteins and vaccines. Pharm. Res. 14, 1431–1436.
Carlander, U., Li, D., Jolliet, O., Emond, C., Johanson, G., 2016. Toward a general physiologically-based pharmacokinetic model for intravenously injected nanoparticles. Int. J. Nanomedicine 11, 625–640.
Cruz, L., Soares, L.U., Dalla Costa, T., Mezzalira, G., da Silveira, N.P., Guterres, S.S., Pohlmann, A.R., 2006. Diffusion and mathematical modeling of release profiles from nanocarriers. Int. J. Pharm. 313, 198–205.
D'Addio, S.M., Saad, W., Ansell, S.M., Squiers, J.J., Adamson, D.H., Herrera-Alonso, M., Wohl, A.R., Hoye, T.R., Macosko, C.W., Mayer, L.D., Vauthier, C., Prud'homme, R.K., 2012. Effects of block copolymer properties on nanocarrier protection from in vivo clearance. J. Control. Release 162, 208–217.
Farace, C., Sánchez-Moreno, P., Orecchioni, M., Manetti, R., Sgarrella, F., Asara, Y., Peula-García, J.M., Marchal, J.A., Madeddu, R., Delogu, L.G., 2016. Immune cell impact of three differently coated lipid nanocapsules: pluronic, chitosan and polyethylene glycol. Sci. Report. 6, 18423.
Fernández-Urrusuno, R., Fattal, E., Rodrigues, J.M., Feger, J., Bedossa, P., Couvreur, P., 1996. Effect of polymeric nanoparticle administration on the clearance activity of the mononuclear phagocyte system in mice. J. Biomed. Mater. Res. 31, 401–408.
Fessi, H., Puisieux, F., Devissaguet, J.P., Ammoury, N., Benita, S., 1989. Nanocapsule formation by interfacial polymer deposition following solvent displacement. Int. J. Pharm. 55, R1–R4.
Frank, L.A., Contri, R.V., Beck, R.C.R., Pohlmann, A.R., Guterres, S.S., 2015. Improving drug biological effects by encapsulation into polymeric nanocapsules. Wiley Interdiscip. Rev. Nanomed. Nanobiotechnol. 7, 623–639.
Garcia, G.M., Oliveira, L.T., Pitta, I.d.R., de Lima, M.d.C.A., Vilela, J.M.C., Andrade, M.S., Abdalla, D.S.P., Mosqueira, V.C.F., 2015. Improved nonclinical pharmacokinetics and biodistribution of a new PPAR pan-agonist and COX inhibitor in nanocapsule formulation. J. Control. Release 209, 207–218.
Goycoolea, F.M., Valle-Gallego, A., Stefani, R., Menchicchi, B., David, L., Rochas, C., Santander-Ortega, M.J., Alonso, M.J., 2012. Chitosan-based nanocapsules: physical characterization, stability in biological media and capsaicin encapsulation. Colloid Polym. Sci. 290, 1423–1434.
Gref, R., Minamitake, Y., Peracchia, M.T., Trubetskoy, V., Torchilin, V., Langer, R., 1994. Biodegradable long-circulating nanospheres. Science 263, 1600–1603.
Gref, R., Luck, M., Quellec, P., Marchand, M., Dellacherie, E., Harnisch, S., Blunk, T., Muller, R.H., 2000. 'Stealth' corona-core nanoparticles surface modified by polyethylene glycol (PEG): influences of the corona (PEG chain length and surface density) and of the core composition on phagocytic uptake and plasma protein adsorption. Colloids Surf. B Biointerfaces 18, 301–313.
Kunz, D., Thurn, A., Burchard, W., 1983. Dynamic light-scattering from spherical-particles. Colloid Polym. Sci. 261, 635–644.
Legrand, P., Barratt, G., Mosqueira, V., Fessi, H., Devissaguet, J.P., 1999. Polymeric nanocapsules as drug delivery systems - a review. Stp Pharm. Sci. 9, 411–418.
Leite, E.A., Vilela, J.M.C., Mosqueira, V.C.F., Andrade, M.S., 2005. Poly-caprolactone nanocapsules morphological features by atomic force microscopy. Microsc. Microanal. 11, 48–51.
Leite, E.A., Grabe-Guimaraes, A., Guimaraes, H.N., Lins Machado-Coelho, G.L., Barratt,

G., Mosqueira, V.C.F., 2007. Cardiotoxicity reduction induced by halofantrine entrapped in nanocapsule devices. Life Sci. 80, 1327–1334.
Lepeltier, E., Bourgaux, C., Couvreur, P., 2014. Nanoprecipitation and the "ouzo effect": application to drug delivery devices. Adv. Drug Deliv. Rev. 71, 86–97.
Ma, P.L., Buschmann, M.D., Winnik, F.M., 2010. Complete physicochemical characterization of DNA/chitosan complexes by multiple detection using asymmetrical flow field-flow fractionation. Anal. Chem. 82, 9636–9643.
Mendes, L.P., Delgado, J.M.F., Costa, A.D.A., Vieira, M.S., Benfica, P.L., Lima, E.M., Valadares, M.C., 2015. Biodegradable nanoparticles designed for drug delivery: the number of nanoparticles impacts on cytotoxicity. Toxicol. in Vitro 29, 1268–1274.
Mora-Huertas, C.E., Fessi, H., Elaissari, A., 2010. Polymer-based nanocapsules for drug delivery. Int. J. Pharm. 385, 113–142.
Mosqueira, V.C.F., Legrand, P., Gref, R., Heurtault, B., Appel, M., Barratt, G., 1999. Interactions between a macrophage cell line (J774A1) and surface-modified poly(D,L-lactide) nanocapsules bearing poly(ethylene glycol). J. Drug Target. 7, 65–78.
Mosqueira, V.C.F., Legrand, P., Gulik, A., Bourdon, O., Gref, R., Labarre, D., Barratt, G., 2001a. Relationship between complement activation, cellular uptake and surface physicochemical aspects of novel PEG-modified nanocapsules. Biomaterials 22, 2967–2979.
Mosqueira, V.C.F., Legrand, P., Morgat, J.L., Vert, M., Mysiakine, E., Gref, R., Devissaguet, J.P., Barratt, G., 2001b. Biodistribution of long-circulating PEG-grafted nanocapsules in mice: effects of PEG chain length and density. Pharm. Res. 18, 1411–1419.
Mosqueira, V.C.F., Leite, E.A., Barros, C.M., Vilela, J.M.C., Andrade, M.S., 2005. Polymeric nanostructures for drug delivery: characterization by atomic force microscopy. Microsc. Microanal. 11, 36–39.
Mosqueira, V.C., Legrand, P., Barratt, G., 2006. Surface-modified and conventional nanocapsules as novel formulations for parenteral delivery of halofantrine. J. Nanosci. Nanotechnol. 6, 3193–3202.
Neves, S.M.P., Ong, F.d.M.P., Rodrigues, L.D., Santos, R.A.D., Fontes, R.S., Santana, R.D.O., 2013. Manual de Cuidados e Procedimentos com Animais de Laboratório do Biotério de Produção e Experimentação da FCF-IQ/USP. São Paulo, FCF-IQ/USP.
Oliveira, L.T., Garcia, G.M., Kano, E.K., Tedesco, A.C., Mosqueira, V.C.F., 2011. HPLC-FLD methods to quantify chloroaluminum phthalocyanine in nanoparticles, plasma and tissue: application in pharmacokinetic and biodistribution studies. J. Pharm. Biomed. Anal. 56, 70–77.
Owens, D.E., Peppas, N.A., 2006. Opsonization, biodistribution, and pharmacokinetics of polymeric nanoparticles. Int. J. Pharm. 307, 93–102.
Panagi, Z., Beletsi, A., Evangelatos, G., Livaniou, E., Ithakissios, D.S., Avgoustakis, K., 2001. Effect of dose on the biodistribution and pharmacokinetics of PLGA and PLGA–mPEG nanoparticles. Int. J. Pharm. 221, 143–152.
Park, J.H., Saravanakumar, G., Kim, K., Kwon, I.C., 2010. Targeted delivery of low molecular drugs using chitosan and its derivatives. Adv. Drug Deliv. Rev. 62, 28–41.
de Paula, C.S., Tedesco, A.C., Primo, F.L., Vilela, J.M.C., Andrade, M.S., Mosqueira, V.C.F., 2013. Chloroaluminium phthalocyanine polymeric nanoparticles as photosensitisers: photophysical and physicochemical characterisation, release and phototoxicity in vitro. Eur. J. Pharm. Sci. 49, 371–381.
Pereira, M.A., Mosqueira, V.C.F., Vilela, J.M.C., Andrade, M.S., Ramaldes, G.A., Cardoso, V.N., 2008. PLA-PEG nanocapsules radiolabeled with 99mTechnetium-HMPAO: release properties and physicochemical characterization by atomic force microscopy and photon correlation spectroscopy. Eur. J. Pharm. Sci. 33, 42–51.
Rodriguez-Emmenegger, C., Jäger, A., Jäger, E., Stepanek, P., Alles, A.B., Guterres, S.S., Pohlmann, A.R., Brynda, E., 2011. Polymeric nanocapsules ultra stable in complex biological media. Colloids Surf. B: Biointerfaces 83, 376–381.
Roy, J., Oliveira, L.T., Oger, C., Galano, J.-M., Bultel-Ponce, V., Richard, S., Guimaraes, A.G., Carneiro Vilela, J.M., Andrade, M.S., Durand, T., Besson, P., Furtado Mosqueira, V.C., Le Guennec, J.-Y., 2015. Polymeric nanocapsules prevent oxidation of core-loaded molecules: evidence based on the effects of docosahexaenoic acid and neuroprostane on breast cancer cells proliferation. J. Exp. Clin. Cancer Res. 34.
Rube, A., Hause, G., Mader, K., Kohlbrecher, J., 2005. Core-shell structure of Miglyol/poly(D,L-lactide)/Poloxamer nanocapsules studied by small-angle neutron scattering. J. Control. Release 107, 244–252.
Shenoy, D., Little, S., Langer, R., Amiji, M., 2005. Poly(ethylene oxide)-modified poly (beta-amino ester) nanoparticles as a pH-sensitive system for tumor-targeted delivery of hydrophobic drugs: part 2. In vivo distribution and tumor localization studies. Pharm. Res. 22, 2107–2114.
Stauch, O., Schubert, R., Savin, G., Burchard, W., 2002. Structure of artificial cytoskeleton containing liposomes in aqueous solution studied by static and dynamic light scattering. Biomacromolecules 3, 565–578.
Torcello-Gomez, A., Wulff-Perez, M., Jose Galvez-Ruiz, M., Martin-Rodriguez, A., Cabrerizo-Vilchez, M., Maldonado-Valderrama, J., 2014. Block copolymers at interfaces: interactions with physiological media. Adv. Colloid Interf. Sci. 206, 414–427.
Vezočnik, V., Rebolj, K., Sitar, S., Ota, K., Tušek-Žnidarič, M., Štrus, J., Sepčić, K., Pahovnik, D., Maček, P., Žagar, E., 2015. Size fractionation and size characterization of nanoemulsions of lipid droplets and large unilamellar lipid vesicles by asymmetric-flow field-flow fractionation/multi-angle light scattering and dynamic light scattering. J. Chromatogr. A 1418, 185–191.
Vicente, S., Goins, B.A., Sanchez, A., Alonso, M.J., Phillips, W.T., 2014. Biodistribution and lymph node retention of polysaccharide-based immunostimulating nanocapsules. Vaccine 32, 1685–1692.
Yang, R., Shim, W.-S., Cui, F.-D., Cheng, G., Han, X., Jin, Q.-R., Kim, D.-D., Chung, S.-J., Shim, C.-K., 2009. Enhanced electrostatic interaction between chitosan-modified PLGA nanoparticle and tumor. Int. J. Pharm. 371, 142–147.
Younes, I., Frachet, V., Rinaudo, M., Jellouli, K., Nasri, M., 2016. Cytotoxicity of chitosans with different acetylation degrees and molecular weights on bladder carcinoma cells. Int. J. Biol. Macromol. 84, 200–207.
Zhao, P., Zheng, M., Yue, C., Luo, Z., Gong, P., Gao, G., Sheng, Z., Zheng, C., Cai, L., 2014. Improving drug accumulation and photothermal efficacy in tumor depending on size of ICG loaded lipid-polymer nanoparticles. Biomaterials 35, 6037–6046.